Reconstruction for proton computed tomography by tracing proton trajectories: A Monte Carlo study

Tianfang Li and Zhengrong Liang[a)]
Departments of Radiology, Computer Science, and Physics and Astronomy, State University of New York at Stony Brook, Stony Brook, New York 11794

Jayalakshmi V. Singanallur and Todd J. Satogata
Department of Physics, Brookhaven National Laboratory, Upton, New York 11973

David C. Williams
The Santa Cruz Institute for Particle Physics, University of California at Santa Cruz, Santa Cruz, California 95064

Reinhard W. Schulte
Department of Radiation Medicine, Loma Linda University Medical Center, Loma Linda, California 92354

(Received 4 August 2005; revised 9 January 2006; accepted for publication 11 January 2006; published 22 February 2006)

Proton computed tomography (pCT) has been explored in the past decades because of its unique imaging characteristics, low radiation dose, and its possible use for treatment planning and on-line target localization in proton therapy. However, reconstruction of pCT images is challenging because the proton path within the object to be imaged is statistically affected by multiple Coulomb scattering. In this paper, we employ GEANT4-based Monte Carlo simulations of the two-dimensional pCT reconstruction of an elliptical phantom to investigate the possible use of the algebraic reconstruction technique (ART) with three different path-estimation methods for pCT reconstruction. The first method assumes a straight-line path (SLP) connecting the proton entry and exit positions, the second method adapts the most-likely path (MLP) theoretically determined for a uniform medium, and the third method employs a cubic spline path (CSP). The ART reconstructions showed progressive improvement of spatial resolution when going from the SLP [2 line pairs (lp) cm^{-1}] to the curved CSP and MLP path estimates (5 lp cm^{-1}). The MLP-based ART algorithm had the fastest convergence and smallest residual error of all three estimates. This work demonstrates the advantage of tracking curved proton paths in conjunction with the ART algorithm and curved path estimates. © *2006 American Association of Physicists in Medicine*. [DOI: 10.1118/1.2171507]

Key words: proton CT, multiple Coulomb scattering, curved proton path, ART algorithm

I. INTRODUCTION

Proton computed tomography (pCT) has several potential advantages in medical applications. Its favorable dose density resolution relationship and its unique image-formation characteristics based on the linear stopping power of charged particles, different from the x-ray attenuation of photons in x-ray CT (xCT), may prove beneficial in medical diagnosis and therapy.[1–3] With the use of medical accelerators with highly stable proton energy output, the proton entry energy would also be known with excellent accuracy and precision. This may be exploited for dose-efficient image reconstruction.[3] For proton radiation treatment, a successful implementation of pCT would avoid the ambiguities of mapping xCT Hounsfield values to electron densities, and would allow verification of patient position and actual dose distribution in the treatment room. Successful integration of pCT with proton therapy may lead to the ultimate form of image-guided three-dimensional (3D) conformal radiation therapy, which has the potential to deliver the optimal dose to any point within the patient and provide arbitrarily shaped inhomogeneous dose distributions as desired. Developing reconstruction algorithms for low-dose pCT imaging techniques is an indispensable prerequisite for the clinical application of pCT.

One difficulty in pCT image reconstruction stems from scattering of the protons inside the body due to the numerous small-angle deflections by nuclear Coulomb fields. Consequently, the use of protons for medical imaging applications has inherent spatial resolution limits.[4] In a recent publication, Zygmanski *et al.*[2] presented a proton CT design based on scattering a penetrating proton beam with a modified upstream modulator that resulted in a linear fluence dependence of the proton beam on the integrated electron density of the object. A prototype scanner tested with the 160 MeV proton beam at the Harvard Cyclotron resulted in improved measurement of stopping power compared to xCT, however, the spatial resolution was significantly affected by multiple Coulomb scattering (MCS).

One potential merit of proton imaging is that the protons can be detected and tracked one-by-one, avoiding the quantum noise of xCT imaging, and making it possible to use reconstruction algorithms based on individual curved trajec-

tories. With current advancements in detector technology for high-energy particle physics[5,6] the location and direction of each proton at the entrance and exit of the patient or phantom can be precisely recorded and its most likely path (MLP) within the object predicted.[4,7] Alternatively, one may use a simpler approximation for the curved path such as cubic splines. The central question of how much pCT reconstruction based on the curved trajectories will improve the spatial resolution of pCT reconstruction and how the improvement relates to the accuracy of single-proton path estimation within the patient have yet to be answered.

In this work, we compare three different estimators for the paths of individual protons inside a given object, including a straight-line path (SLP) approximation, the MLP, and a cubic spline path (CSP), when used with an algebraic reconstruction technique. The performance of the different path reconstruction techniques were compared using pCT data sets generated with an application based on the GEANT4 Monte Carlo (MC) simulation toolkit.[8] It is shown that reconstruction based on curved paths provides a significantly better spatial resolution in the reconstruction of a mathematical phantom than the straight-line path reconstruction.

II. METHODS AND MATERIALS

A. Radon transform presentation of proton CT

The principle of proton CT reconstruction of the relative electron density based on measurement of proton energy has been described in detail previously.[1,3] In short, knowledge of the entry and exit energy of a proton allows estimating the integrated (projected) relative electron density with respect to a reference medium (e.g., water) along the proton path L

$$\int_L \eta(r)dr = K\int_{E_{\text{out}}}^{E_{\text{in}}} \frac{dE}{S(E)}, \tag{1}$$

where E_{in} is the incident proton energy and E_{out} is the proton energy after traversing through the object, $S(E)$ is the proton stopping power, and K is a constant. The proton stopping power is described by the Bethe-Bloch formula.[9] The latter requires the mean excitation potential of the medium, for which the value of water (75 eV)[10] was used in this work. With Eq. (1), the integrated relative electron density (on the left side) can be calculated by integrating the inverse stopping power using the knowledge of in- and out-going proton energy (on the right side). In order to simplify the calculations, we used a simplified form of the Bethe-Bloch formula,[3] which neglects density- and shell-correction terms. Equation (1) resembles the format of the Radon transform used in xCT if the proton path L is assumed as a straight line. The right side of Eq. (1) represents the measured path integral. Reconstruction of pCT is to invert the path integral for the unknown relative electron density distribution $\eta(r)$. Unlike the inversion in xCT, the exact path in pCT is unknown due to the presence of MCS and must, therefore, be estimated.

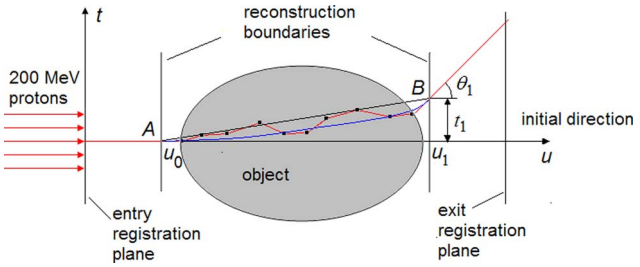

FIG. 1. Scattering and simulation geometry used throughout this work. The third dimension is neglected. The path of protons traveling inside an object is determined by a multitude of individual scattering events leading to a zigzag path (red). Both the position and direction of entry and exit proton are registered. Given the boundary of the reconstruction region, the intersecting points A and B of a proton with the object can be obtained assuming there is no scattering medium between registration planes and reconstruction boundaries. While the intersecting points are sufficient to estimate the straight line path (black) of the proton, additional knowledge of the entry and exit directions permits estimation of the most likely path (blue line).

B. Proton path estimates

Since protons undergo MCS, the path of each proton in the object deviates from its initial direction as illustrated in Fig. 1. Most of the scattering events contribute only a small deflection from the proton path but larger individual deflections occur as well, contributing to a long tail of the angular distribution of outgoing protons. These large scattering-angle events due to elastic nuclear interactions can be excluded by performing three-sigma cuts on the outgoing scattering angles. In addition to MCS, inelastic nuclear interactions also contribute to the scattering of protons. Although these events are much less frequent, they can also produce relatively large angular scattering events. However, as these events are usually associated with a large energy loss they usually do not exit the object, or if they do they can be successfully removed from pCT data by performing three-sigma cuts on the outgoing energy.[3]

Given the entry and exit position of a proton, any proton path within the object has a certain likelihood that can, in principle, be calculated based on an appropriate MCS theory. Molière's small-angle scattering theory of MCS[11,12] is generally considered appropriate but due to its mathematical complexity only its Gaussian approximation is suitable to derive the conditional probability density distributions of displacement and angle inside the object.[7,13] Both the position and direction of each entry and exit proton can be measured accurately by a position- and angle-sensitive detector system. With this information, and after excluding large-angle scattering events, it is possible to derive estimates of the proton paths through the phantom with varying degrees of accuracy.

1. Straight-line path

A straight line path (SLP) is the simplest, though naïve, estimation of the proton path. It is defined by the line between the intersections of the entry and exit path lines of each proton with the boundary of the reconstruction area, i.e., points "*A*" and "*B*" in Fig. 1. For a proton beam incident

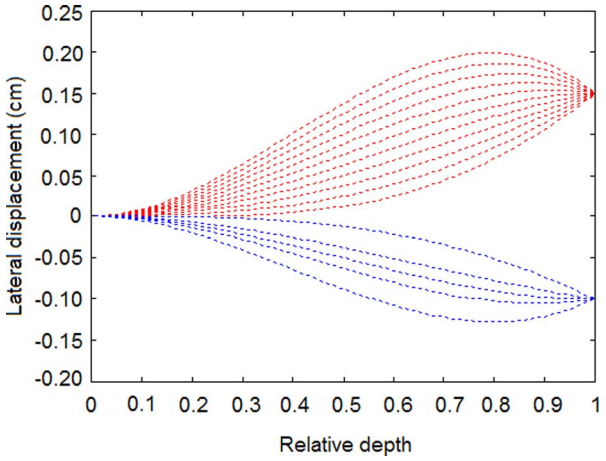

FIG. 2. Examples of MLPs for protons in water entering the u-t plane at $t=0$ and with two different exit displacements t_1 (0.15 mm, −0.10 mm) and several different exit angles θ_1. The depth coordinate is given as a fraction of the exit depth. Note that the same SLP applies to each group of MLPs.

on a homogeneous and isotropic scattering medium, the straight line is the most likely path if the protons are uniformly distributed in different directions (uniform distribution of the entry angle).

2. Most-likely path

The internal paths of protons follow a certain probability distribution. If the object has a homogeneous electron density over the entire scan region and both entry and exit points and directions are known, the MLP, i.e., the most likely of all possible trajectories given entry and exit positions and angles can be analytically derived.[7] To simplify matters, we consider proton trajectories projected into the reconstruction plane (u-t plane in Fig. 1). Given the position and direction of an incoming proton at point "A" $(u_0, t_0, \theta_0=0)$ and the exit position and direction at point "B" (u_1, t_1, θ_1), the MLP $t(u)$ in a homogenous object is given by Eq. (14) in[7]

$$t(u) = (AE - BD)/(AC - B^2), \tag{2}$$

where A, B, C, D, and E are abbreviations for terms that depend on the available proton track information and initial proton energy and are described by Eqs. (15)–(27) in Ref. 7. Note that the six integrals of Eqs. (22)–(27) in Ref. 7 for calculating A, B, C, D, E contain the quantity $1/\beta^2p^2$, i.e., the product of proton speed relative to the velocity of light and proton momentum, which vary with the depth u because of the change of the kinetic energy during the proton traversal through the object. As described in Ref. 7, their relation to u can be described by a five-degree polynomial, $1/\beta^2p^2=\Sigma_{i=0}^{5} a_i u^i$, where the parameters a_i were selected as those in Ref. 7, which were obtained by curve fitting of the results from a GEANT4 MC simulation data for 200-MeV protons traversing a uniform water phantom. Specifically, $a_0=7.507e-4$, $a_1=3.320e-5$, $a_2=-4.171e-7$, $a_3=4.488e-7$, $a_4=-3.739e-8$, and $a_5=1.455e-9$, where the units are c^2/MeV divided by various powers of cm. Figure 2 shows several examples of the most-likely paths calculated by Eq. (2) for protons with initial kinetic energy of 200 MeV traveling though 20 cm of water, given the same entry position and direction and two different t displacements and several deflection angles at each t displacement. Similar results can be found in Ref. 7.

3. Cubic spline path

The MLP can be considered as the best statistical estimate of the internal path of a proton traveling through a uniform medium. Since the positions and tangential directions (or derivatives) of the proton at the entrance and exit are known, an alternative and mathematically simpler way to estimate the proton path is to fit the two end points with a smooth polynomial. Here, a cubic spline was used, which leads to the cubic spline path or CSP estimate

$$t'(u) = a + bu + cu^2 + du^3, \tag{3}$$

where the coefficients a, b, c, and d are determined by matching the positions and slopes of the spline function at the beginning and end points, i.e., points "A" and "B" in Fig. 1, to the given data.

The SLP, MLP, and CSP estimators of the proton paths were incorporated into an iterative reconstruction algorithm as described below.

C. ART image reconstruction

We assume that each proton's entry and exit angle and position in the entry and exit registration planes are provided along with the energy loss in the pCT scan, therefore individual proton paths can be estimated with the methods described in Sec. II B. For the curved (most-likely and cubic spline) paths, the filtered or convolution back projection reconstructions commonly used in xCT are no longer feasible and a different reconstruction technique must be used. The algebraic reconstruction technique (ART),[14] a procedure based on iterative relaxation of a system of equations, with each equation representing the projection of the discretized relative electron density along a single path, has proven suitable in this case.[15]

In this application, we have implemented the ART algorithm as described previously.[16,17] It is assumed that a total of N projections of the relative electron density function is available. The object slice to be reconstructed is digitized into $n \times n$ pixels, and the relative electron density is expressed as a n^2-dimensional vector. Specifically, the iterative ART algorithm is expressed as

$$\eta^{(k+1)} = \eta^{(k)} + \lambda^{(k)} \frac{\mathbf{H}^T[p - \mathbf{H}(\eta^{(k)})]}{\mathbf{H}^T[\mathbf{H}(\mathbf{1})]}, \tag{4}$$

where $\mathbf{H}[.]$ is the operator for forward projection, symbol T denotes the transpose operation, and $\mathbf{H}^T[.]$ is the operator for backward projection. The denominator is the normalization constant relating to the projection operations. The notation η denotes the relative electron density vector to be reconstructed, and the vector p is the projection of the relative electron density derived from the N measured energy loss values using Eq. (1). Index k is the iteration number, and λ^k

is a relaxation factor for the kth update, which needs to be chosen for optimum performance.[16,17] The forward and backward projections are performed by weighted summation using the intersecting lengths of each path with the associated pixel on that path in the object. Note that this procedure can be performed for any path estimate. The iterative reconstruction process is stopped when the difference of successive iterations is less than a limit (e.g., 0.1%) or a maximum iteration number is reached.

D. Monte Carlo simulation

The pCT data used in this work for comparison of the reconstruction with different path estimates were obtained by MC simulations using an application created with the GEANT4 toolkit, a computer library for the simulation of particles interacting with matter originally developed for high-energy physics.[8] More recently GEANT4 has also been used as a simulation tool in medical physics applications. In particular, it has been shown to be useful for proton treatment plan calculations.[18,19]

For this work, the physics processes of the GEANT4 application were configured as per GEANT4 example number two with the standard (high energy) energy loss, multiple scattering processes, and the parametrized hadronic interaction model for protons. A stepping range limit of 2 mm was employed. To improve the accuracy in this application, the hadronic energy loss table was initialized with 2000 steps up to a maximum kinetic energy of 500 MeV. GEANT4 uses a non-Gaussian model of multiple scattering based on the transport theory from Lewis[20] that attempts to accurately characterize MCS not only at small angles but also the tails from large-angle scattering. Secondary protons produced by inelastic nuclear interactions were included in the simulation.

A phantom was used in the pCT scan simulation, which is shown in Fig. 3. For characterization of the spatial resolution, it contains two sets of line patterns (strips) embedded within a water phantom with an elliptical cross section simulating a human head with a longitudinal diameter of 16 cm, a transverse diameter of 14 cm, and a height of 20 cm. The first set of strips has ICRU-compact bone density,[21] while the second set comprises strips with air density. The line-pair density each set of strip patterns are 2, 2.5, 3, 3.5, 4, 4.5, 5, and 6 line pairs per cm (lp cm^{-1}). The elliptical water phantom is surrounded by a 1 cm thick shell of ICRU compact bone density, simulating the human skull.

Proton beams of 200 MeV were generated with GEANT4 (version 6.2) for the pCT scan with 50 000 protons randomly distributed along the t axis over a length of 24 cm at each projection angle. The beams were idealized fan beams confined to the u-t plane (Fig. 1). A total of 180 projections was acquired, evenly distributed over 360 deg. The dose to the center of the phantom was estimated using the formalism to determine the proton dose to a circular water phantom described previously.[3] To adapt this formalism to the present phantom, the bone shell was converted to a shell of 1.9 cm water-equivalent thickness (WET), and the resulting uniform ellipse (ignoring inserts) was converted to a circular disk of identical area with a WET of 8.8 cm and a height of 1 mm. The dose at the center of the disk resulting from the 180 projections with 50 000 protons per projection was calculated to be 3.5 mGy. The relevant entry and exit data of each proton including the position in the (u,t) entry plane ($u=0$ cm), exit energy, and position in the (u,t) exit plane ($u=30$ cm), see Fig. 1, and exit direction projected onto the (u,t) plane, were stored in the computer. The position and direction data were used to calculate the path estimates for each proton within a "virtual" circular object boundary of 22 cm diameter. One should note that due to MCS, the exiting protons were no longer confined to the u-t plane. In order to limit the reconstruction to a 2D case, the coordinate in the direction vertical to the u-t plane was set to zero. The energy information for each proton was used to compute the energy lost in the object as well as the integrated relative electron density along each proton path using Eq. (1).

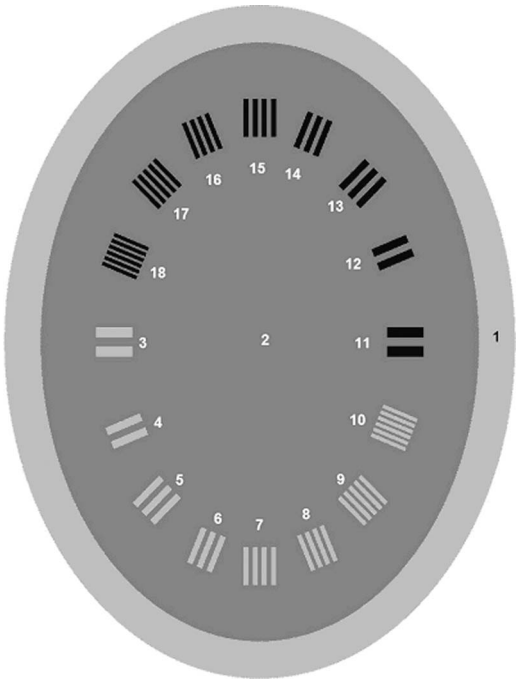

FIG. 3. Elliptical phantom consisting of an outer shell with bone density (1), an elliptical interior of water density (2), and two sets of strip patterns with either bone density (white) or air density (black). The strip densities of the patterns (listed by number) are: 2 lp cm^{-1} (3, 11), 2.5 lp cm^{-1} (4, 12), 3 lp cm^{-1} (5, 13), 3.5 lp cm^{-1} (6, 14), 4 lp cm^{-1} (7, 15), 4.5 lp cm^{-1} (8, 16), 5 lp cm^{-1} (9, 17), and 6 lp cm^{-1} (10, 18).

III. RESULTS

A. Comparison of path estimates

In order to demonstrate how closely the different path estimates matched the simulated proton paths, a pencil beam of protons incident on a uniform 20 cm × 20 cm × 20 cm rectangular volume of water was simulated with the GEANT4 application. Protons of 200 MeV initial kinetic energy were generated, and their paths (lateral and angular displacement versus depth) were recorded at 1-mm intervals for a total of 200 steps. For each proton, the SLP, MLP, and CSP estimates

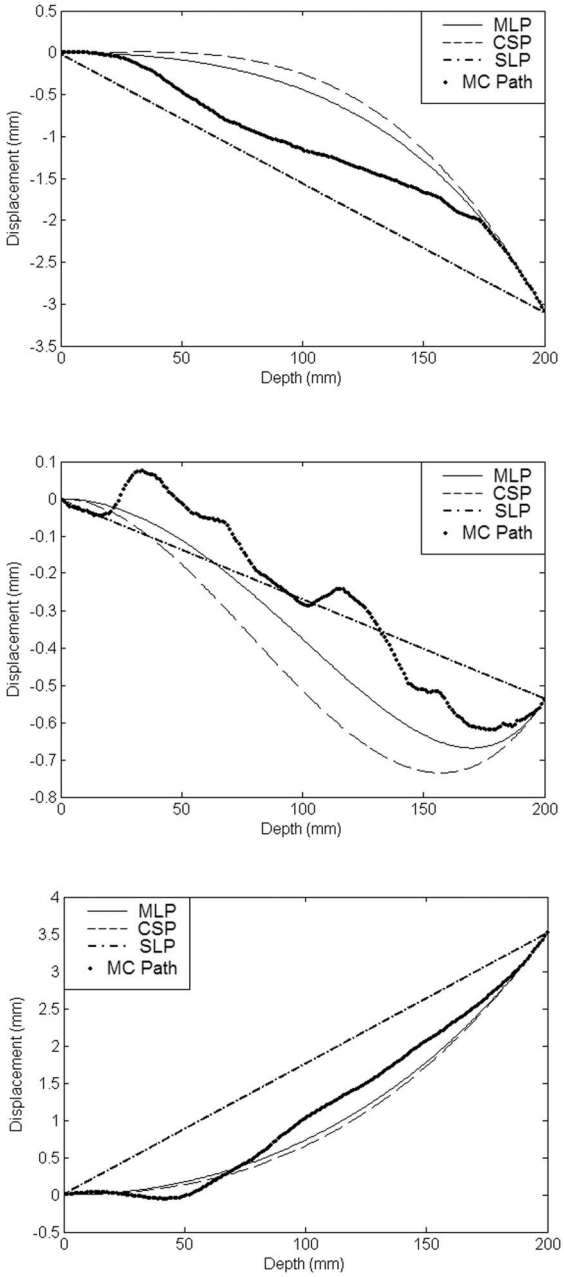

FIG. 4. Three examples of MC-simulated proton paths in water and their estimated SLP, MLP, and CSP.

of the 2D-projected paths were calculated based on the exit information of the simulated events at a depth of 20 cm. Protons undergoing inelastic nuclear interactions and those undergoing large-angle scattering (3D-exit angle >0.1 rad) were excluded from the analysis as these were also suppressed in the pCT reconstruction of the elliptical phantom.

A total of 10 000 proton histories were simulated and 9250 histories were found appropriate for analysis. Figure 4 shows three such estimated paths, calculated as described in Sec. II B. The entry and exit positions and angles of these events are listed in Table I.

The root mean square (RMS) deviation of the lateral displacement (t) in the projection plane between each path estimate and the MC-simulated internal path is shown in Fig. 5 as a function of depth in the water layer (u). As expected, for all three path estimates the largest RMS deviation is seen about half-way between entry and exit depth where the paths are farthest from the known entry and exit points. Comparing the different path estimates, the smallest RMS deviation is provided by the MLP estimate (about 0.5 mm in the central region). The RMS of the CSP estimate is less than 10% larger for this phantom geometry. On the other hand, the RMS of the SLP estimate exceeds 1 mm in the central region, being about two times larger than that of the curved path estimates.

TABLE I. Entry and exit positions and directions of three arbitrarily selected proton events (200 MeV initial energy), of which the simulated paths and estimated paths are plotted in Fig. 4.

History	t_0 (mm)	u_0 (mm)	θ_0 (radian)	t_1 (mm)	u_1 (mm)	θ_1 (radian)
Proton 1	0	0	0	−3.09	200	−5.72e-2
Proton 2	0	0	0	−0.54	200	9.78e-3
Proton 3	0	0	0	3.51	200	4.40e-2

B. Comparison of ART reconstructions

1. Qualitative comparison

The simulated pCT data of the elliptical phantom shown in Fig. 3 were reconstructed by the ART algorithm using the different path estimates as defined in Sec. II B. In the ART reconstruction, the corresponding equations describing each of the path estimates were implemented through the forward projection and backward projection processes to incorporate the individual proton paths [Eq. (4)]. A relaxation factor of $\lambda=1$ and a pixel size of 0.25 mm was used for all reconstructions. The initial image was set to be zero, and satisfactory reconstructions were obtained after 120 iterations in all cases (see "convergence speed" below). The ART reconstruction results for SLP, CSP, and MLP estimates are shown in Fig. 6.

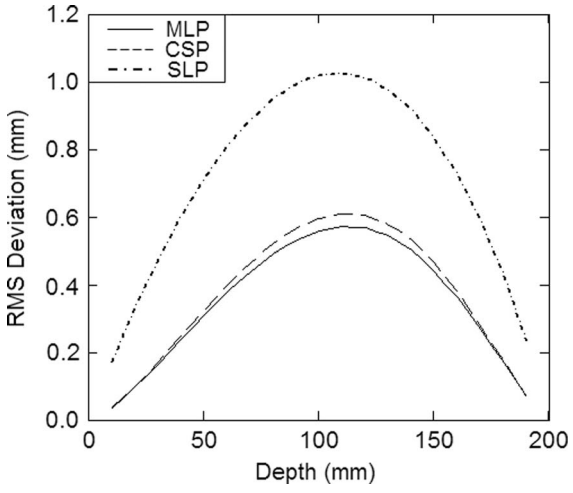

FIG. 5. Comparison of the RMS deviation of the lateral displacement in the projection plane between each path estimate and the MC-simulated internal path as a function of depth in a 20-cm water layer

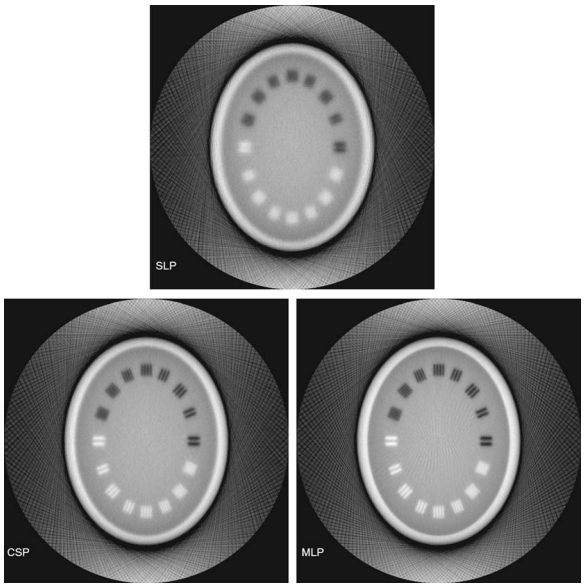

FIG. 6. Reconstructions of the elliptical phantom by the ART algorithm using SLP (top) CSP (bottom left) and MLP (bottom right) estimates.

It is seen that the SLP-based reconstruction (top of Fig. 6) shows a considerable loss of spatial resolution, with a resolution of about 2.5 lp cm^{-1} for the air-density pattern and about 2 lp cm^{-1} for the bone-density pattern. In comparison, tracing the proton paths with MLP or CSP for the ART reconstruction demonstrates observable improvement in spatial resolution to about 5 and 4.5 lp cm^{-1} for the air-density pattern and the bone-density patterns, respectively. The ART reconstruction with either the MLP estimate (right bottom of Fig. 6) or the CSP estimate (left bottom of Fig. 6) seems to generate similar image quality.

2. Comparison using line profile plots

To evaluate the reconstructions shown in Fig. 6 in a more quantitative way, an "average density profile" of pattern 15 of the phantom (air density, 4 lp cm^{-1}) was produced by taking an average over 30 consecutive horizontal profiles through the center of the pattern. The averaging was done to reduce the image degradation by the presence of noise.

Figure 7 shows the average profile plots for the three different path estimates, which demonstrates how the spatial resolution is affected by the quality of the path estimate. In particular, it can be seen that the MLP-based algorithm exceeds the CSP-based algorithm in resolution, despite similar image quality in Fig. 5.

3. Convergence speed and residual error

The convergence property of the ART algorithm was compared for the three different path estimates. Figure 8 shows the sum of squared residual errors between the projection of the kth iteration of the relative electron density vector and the "ideal" simulated projection vector versus the iteration number k. The number of projections used in this calculation was 5000 per angle, for a total of 180 angles. For all three

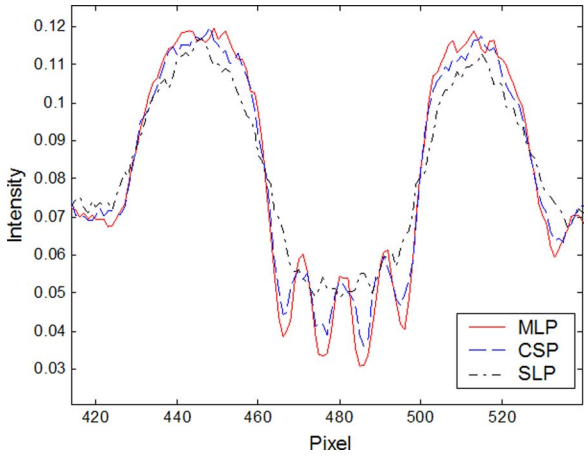

FIG. 7. Average profiles through the top pattern of the reconstructed elliptical phantom of Fig. 3 for the three different path estimates.

path estimates, the algorithm converges to a solution. Further, it is observed that the MLP estimate makes the reconstruction converge faster and leads to a smaller residual error than either CSP or SPL path estimates.

IV. DISCUSSIONS AND CONCLUSIONS

As shown previously,[1,2] multiple Coulomb scattering of protons inside the image object limits the spatial resolution of pCT. In a previous report we suggested that the spatial resolution of the reconstructed pCT image can be improved by using estimators for the curved trajectories instead of a straight-line approximation.[15] In the present work, we compared three different estimators for the paths of individual protons inside a given object, including a straight-line path approximation, the most likely path, and a cubic spline path, in conjunction with an ART algorithm. In order to compare the performance of the different path estimators, we chose to use a mathematical phantom model similar in shape and composition to the head phantom suggested by Shepp and

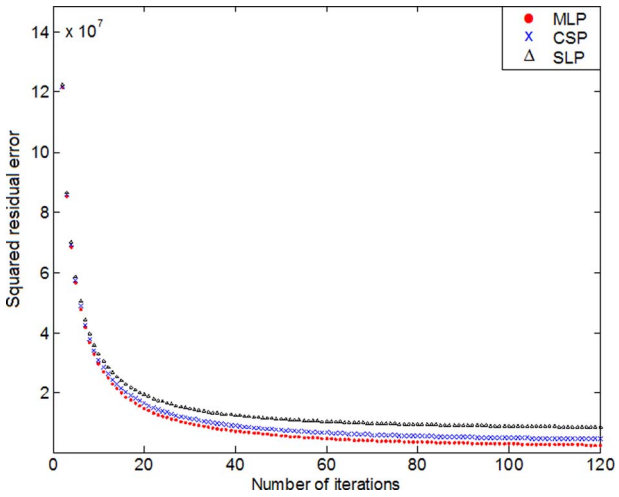

FIG. 8. Convergence speed and squared residual error for the three different path estimates.

Logan,[22] but specifically designed to reveal small differences in spatial resolution. pCT projection data of this phantom were produced with the GEANT4 simulation tool. The advantage of this approach is that the performance of a new and expensive imaging technology can be tested and optimized before it is built.

Our comparison of simulated paths with the SLP, CSP, and MLP estimators in a homogeneous water phantom showed that the RMS difference between these estimators and the "real" (simulated) paths are typically in the 0.5–1 mm range in the center of a water phantom of 20 cm diameter. The largest RMS difference was observed for the SLP, while the RMS difference of the MLP and CSP differed by not more than 10%. This shows that the CSP, which is computationally simpler, is a good approximation of the MLP. Nevertheless, it should be stressed that the MLP provided the highest spatial resolution (Fig. 7) and fastest convergence of the three path estimates (Fig. 8).

One should mention that the path estimators in this work were based on a homogenous water medium and a Gaussian approximation of the MCS statistical distributions.[7] Both assumptions conflict with the real situation where tissue inhomogeneities and individual large-angle scattering events (i.e., the "tails" of the distribution) certainly will affect the individual paths. Scattering theories such as Molière's predict that the scattering distribution of angle and displacement depends both on the density of the material and its atomic number composition.[23] In general, a larger spread of the proton paths can be expected in denser tissues such as bone when compared to soft tissues of near-water density. While large-angle scattering events were eliminated in our reconstruction by performing cuts based on the exit direction of individual protons, the effect of tissue inhomogeneities was not taken into account. This can explain the facts that the spatial resolution of the tissue phantom reconstruction did not reach the level predicted by the RMS deviation of the path estimators (Fig. 5) and the resolution of the bone-density patterns was worse than that of the air-density patterns (Fig. 6).

We chose the ART algorithm for reconstructing pCT images instead of the convolution or filtered back projection (FBP) algorithms commonly used in xCT. These algorithms are not suitable for curved path reconstruction. In the FBP reconstruction, an interpolation step to map the data onto regular grids in the sinogram space has to be performed first, which further reduces the spatial resolution. With ART, curved proton paths can be traced individually during the forward and backward projection cycles, which makes it the preferred reconstruction algorithm for pCT. Another advantage of ART is that it can be readily applied for reconstruction in three dimensions.[14] Although we have limited our study to a 2D reconstruction with 2D fan beams, a more realistic scenario would include proton beams with cone-beam geometry. Since protons are scattered independently in any direction perpendicular to their path, MLPs and CSPs can also be calculated in the plane orthogonal to the one considered in our study (the u-t plane), and thus 3D paths can be derived by combining the paths from each plane.

The disadvantages of ART include its higher computational cost[24] (e.g., 12 hours computation time for the MLP reconstruction shown in Fig. 6) and the fact that its performance will depend on the choice of the relaxation factor and the particular image type.[15,16] More research is clearly needed to study the accuracy of ART in the determination of relative electron density, which is important for the application of pCT in proton therapy planning.

One possibility of further improving the spatial resolution of the ART reconstruction method is to eliminate proton histories with relatively large statistical variation of the deviation from their estimated path using the information on entry and exit position and angle available. This would correspond to an effective collimation of the protons at the expense of a larger number of histories needed for the same density resolution and therefore an increased patient dose.

An additional improvement of the MLP estimation for inhomogeneous objects (such as the human body) may still be achievable by including the MC simulation into the iterative forward and backward projection cycles rather than estimating the MLP analytically. For example, both the path estimation and the image reconstruction can be iteratively updated with MC simulation in an interleaved manner as shown for an emission tomography geometry.[25] Furthermore, if the path probability distribution can be estimated given the entrance and exiting positions as well as the energy and other measurements, then the sinogram can be determined by tracing each proton through the body with the weights given by the path probability distribution, rather than tracing it along the MLP. A statistical reconstruction that is built on a statistical model and distribution of the proton event measurement may help to improve the performance of pCT further. However, these approaches will further increase the computational cost. With advancements in computing speed and algorithms, the reconstruction time may be substantially reduced by both hardware and software improvements. For example, tenfold improvements in reconstruction speed have already been realized with the use of optimized (GPU) hardware architectures in consumer, personal computer (PC) graphics cards.[26,27] Large-scale parallel computing with an inexpensive personal computer PC cluster is another attractive alternative for reconstruction performance improvements.

ACKNOWLEDGMENTS

This work was supported in part by the NIH National Cancer Institute under Grant No. CA82402. The authors would like to thank all colleagues (H. Sadrozinski, S. Peggs, K. Mueller, Andrew Wroe) of the pCT collaboration for their encouragement and invaluable advice.

[a]Author to whom correspondence should be addressed; electronic mail: jzl@mil.sunysb.edu

[1]K. Hanson, J. Bradbury, T. Cannon, R. Hutson, D. Laubacher, R. Macek, M. Paciotti, and C. Taylor, "Computed tomography using proton energy loss," Phys. Med. Biol. **26**, 965–983 (1981).

[2]P. Zygmanski, K. P. Gall, Monroe S. Z. Rabin, and S. J. Rosenthal, "The measurement of proton stopping power using proton-cone-beam computed tomography," Phys. Med. Biol. **45**, 511–528 (2000).

[3]R. Schulte, V. Bashkirov, M. Klock, T. Li, A. Wroe, I. Evseev, D. Williams, and T. Satogata, "Density resolution of proton computed tomography," Med. Phys. **32** 1035–1046 (2005).
[4]U. Schneider and E. Pedroni, "Multiple Coulomb scattering and spatial resolution in proton radiography," Med. Phys. **21**, 1657–1663 (1994).
[5]R. Schulte, V. Bashkirov, T. Li, Z. Liang, K. Mueller, J. Heimann, L. R. Johnson, B. Keeney, H. Sadrozinski, A. Seiden, D. Williams, L. Zhang, Z. Li, S. Peggs, T. Satogata, and C. Woody, "Conceptual design of a proton computed tomography system for applications in proton radiation therapy," IEEE Trans. Nucl. Sci. **51**, 866–872 (2004).
[6]H. F.-W. Sadrozinski, V. Bashkirov, M. Bruzzi, 1, L. R. Johnson, B. Keeney, G. Ross, R. W. Schulte, A. Seiden, K. Shahnazi, D. C. Williams, and L. Zhang, "Issues in proton computed tomography," Nucl. Instrum. Methods Phys. Res. A **511**, 275–281 (2003).
[7]D. Williams, "The most likely path of an energetic charged particle through a uniform medium," Phys. Med. Biol. **49**, 2899–2911 (2004).
[8]S. Agostinelli, J. Allison, K. Amako, J. Apostolakis, H. Araujo, P. Arce, M. Asai, D. Axen, S. Banerjee, G. Barrand *et al.*, "GEANT4 – A simulation toolkit," Nucl. Instrum. Methods Phys. Res. A **506**, 250–303 (2003).
[9]H. Bichsel, "Charged particle-matter interactions," *Atomic Molecular and Optical Physics Handbook*, edited by G. W. F. Drake (American Institute of Physics Press, Woodbury NY, 1996), Chap. 89, pp. 1032–1044.
[10]National Institute for Standards and Technology, Material Composition database, Online Available: http://www.physics.nist.gov/cgi-bin/Star/compos.pl?ap [September 2004]. National Institute of Standards and Technology, Gaithersburg, MD.
[11]G. Molière, "Theorie der Streuung schneller geladener Teilchen. I. Einzelstreuung am abgeschirmten Coulomb-Feld," Z. Naturforsch. A **2A**, 133–145 (1947).
[12]G. Molière "Theorie der Streuung schneller geladener Teilchen. II. Mehrfach- und Vielfachstreuung," Z. Naturforsch. A **3A**, 78–97 (1948).
[13]G. Molière, "Theorie der Streuung schneller geladener Teilchen. III. Die Vielfachstreuung von Bahnspuren unter Berücksichtigung der statistischen Kopplung," Z. Naturforsch. A **10A**, 177–211 (1955).
[14]G. T. Herman, *Image Reconstruction from Projections. The Fundamentals of Computerized Tomography*, edited by W. Rheinboldt (Academic Press, Orlando FL, 1980), pp. 180–204.
[15]T. Li and Z. Liang, "Reconstruction with most likely trajectory for proton computed tomography," Proc. SPIE Medical Imaging: Image Process. **5370**, 2067–2074 (2004).
[16]K. M. Hanson, "POPART - Performance Optimized Algebraic Reconstruction Technique" in Visual Communications and Image Processing, edited by T. Hsing, Proc. SPIE **1001**, 318–325 (1988).
[17]K. M. Hanson, "Optimization of the constrained Algebraic Reconstruction Technique for the performance of a variety of visual Tasks," *Information Processing in Medical Imaging*, edited by D. A. Ortendahl and J. Llacer (Wiley-Liss, New York, 1990), pp. 45–57.
[18]H. Jiang and H. Paganetti, "Adaptation of GEANT4 to Monte Carlo dose calculations based on CT data," Med. Phys. **31**, 2811–2818 (2004).
[19]H. Paganetti, H. Jiang, E. Rietzel, J. Adams, and G. T. Chen, "The potential of four-dimensional Monte Carlo dose calculation for investigating organ motion effects with high temporal resolution," Int. J. Radiat. Oncol., Biol., Phys. **60**, 942–950 (2004).
[20]H. W. Lewis, "Multiple scattering in an infinite medium," Phys. Rev. **78**, 526–529 (1950).
[21]International Commission on Radiation Units and Measurements, "*Tissue Substitutes in Radiation Dosimetry and Measurements*," ICRU Report No. 44 (ICRU, Bethesda, MD, 1989).
[22]L. A. Shepp and B. F. Logan, "The Fourier reconstruction of a head section," IEEE Trans. Nucl. Sci. **21**, 21–43 (1974).
[23]B. Gottschalk, A. M. Koehler, R. J. Schneider, J. M. Sisterson, and M. S. Wagner, "Multiple Coulomb scattering of 160 MeV protons," Nucl. Instrum. Methods Phys. Res. B **74**, 467–490 (1993).
[24]G. T. Herman and A. Lent, "Iterative reconstruction algorithms," Comput. Biol. Med. **6**, 273–294 (1976).
[25]Z. Liang, R. Jaszczak, E. Coleman, and V. Johnson, "Simultaneous reconstruction, segmentation, and edge enhancement of relatively piecewise continuous images with intensity-level information," Med. Phys. **18**, 394–401 (1991).
[26]J. Wen, Z. Wang, B. Li, T. Li, and Z. Liang, "Speedup of an analytical algorithm for non-uniform attenuation correction using PC video/graphics card architecture," IEEE Trans. Nucl. Sci. **51**, 726–732 (2004).
[27]Z. Wang, G. Han, T. Li, and Z. Liang, "Speedup OS-EM image reconstruction by PC graphics card technologies for quantitative SPECT with varying focal-length fan-beam collimation," IEEE Trans. Nucl. Sci. **52**, 1274–1280 (2005).